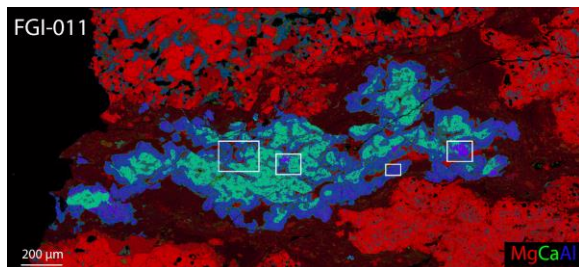


**MINERALOGY AND PETROLOGY OF FINE-GRAINED CALCIUM-ALUMINUM-RICH INCLUSIONS FROM THE REDUCED CV3 CHONDRITE THIEL MOUNTAINS 07007.** C. J. Anderkin<sup>1,2</sup>, J. Han<sup>1,3</sup>, C. Park<sup>4</sup>, and L. P. Keller<sup>3</sup>. <sup>1</sup>Lunar and Planetary Institute, USRA, 3600 Bay Area Boulevard, Houston, Texas, 77058 USA, <sup>2</sup>Department of Geological Sciences, University of Florida, 1843 Stadium Road, Gainesville, FL 32612, USA (anderkinc@ufl.edu), <sup>3</sup>ARES, XI3, NASA Johnson Space Center, 2101 NASA Parkway, Houston, TX 77058, USA, <sup>4</sup>Division of Earth-System Sciences, Korea Polar Research Institute, 26 Songdomirae-ro, Yeosu-gu, Incheon 21990, South Korea.

**Introduction:** Calcium-Aluminum-rich inclusions (CAIs) are among the oldest Solar System solids, and studies of these objects have played an essential role in developing an understanding of chemical and physical processes that initiated and characterized key events related to the Solar System's formation and evolution [1]. CAIs occur as  $\mu\text{m}$ - to  $\text{cm}$ -sized inclusions in chondritic meteorites, particularly in carbonaceous chondrites, and consist of various refractory silicate and oxide phases (e.g., melilite, spinel, Al-Ti-rich diopside, hibonite, and corundum) that are predicted by thermodynamic models to be among the first solids to condense from a cooling gas of solar composition [2]. Fine-grained CAIs (FGIs) are important samples to probe volatility-driven condensation processes in the solar nebula, because they have escaped thermal processes (e.g., melting) experienced by coarse-grained CAIs [3]. In order to explore the primary nebular history of FGIs, a detailed mineralogical and petrologic study is necessary. In this research effort, we constrained the mineralogy and petrology of two CAIs 07-10 and -11 from the reduced CV3 chondrite Thiel Mountains (TIL) 07007, with the aim of evaluating their provenance as nebular condensates.

**Methods:** Our initial survey of CAIs from TIL 07007 was conducted using JEOL JXA-8530F electron microprobe at Korea Polar Research Institute. Two CAIs 7-10 and -11 selected for this study were analyzed in detail using JEOL 7600F field emission scanning electron microscope and JEOL JXA-8530F electron microprobe at NASA Johnson Space Center.



**Fig. 1.** False color x-ray map in Mg (red), Ca (green), and Al (blue) of FGI 7-11. Boxes indicate imaged areas shown in Figs. 2-4.

**Results I. FGI 7-11** is a zoned object with a core-mantle structure, rimmed by diopside (Fig. 1). In this analysis, the core and mantle are dealt with separately,

and an additional mineralogical outline of spinel-rich nodules present in FGI 7-11 is provided here.

**Core:** The core of FGI 7-11 is dominated by gehlenitic melilite ( $\text{Åk}_{6.7-9.6}$ ) that contains minor anhedral spinel and accessory perovskite and grossmanite (Fig. 2). Melilite is often greater than  $30 \mu\text{m}$  in size, which contrasts the average grain size of spinel within the core, which, on average, is approximately  $3 \mu\text{m}$  in size. Spinel is near end-member  $\text{MgAl}_2\text{O}_4$ , and there is little to no compositional variation in spinel throughout the CAI core ( $\text{Mg}\# = 99.0-99.8$ ).

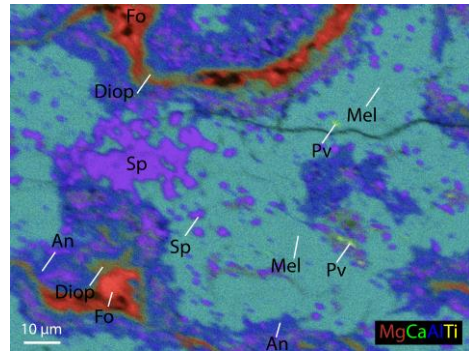


**Fig. 2.** False color x-ray map in Mg (red), Ca (green), Al (blue), and Ti (yellow) of FGI 7-11 core. Sp = spinel, Mel = melilite, Fo = forsterite, An = anorthite, Pv = perovskite, Diop = diopside.

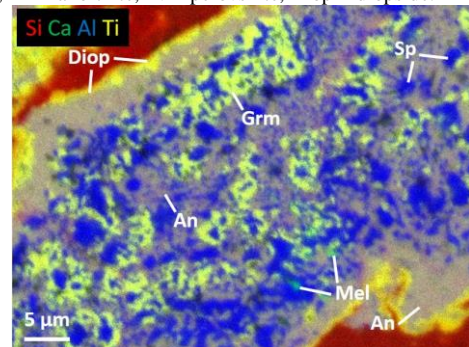


**Fig. 3.** False color x-ray map in Si (red), Ca (green), Al (blue), and Ti (yellow) of FGI 7-11 mantle. Grm = grossmanite.

**Mantle:** The dominant mineral in the mantle is anorthite ( $\text{An}_{99.3-99.9}$ ), followed by grossmanite and spinel with lesser melilite (Fig. 3). Anorthite generally encloses spinel and grossmanite here, and grains are on average around  $4 \mu\text{m}$  wide. Grossmanite grains are widespread, but are often between  $0.5$  and  $1 \mu\text{m}$  in size, and aggregates of these grains are intergrown with

spinel. Spinel is often found as ovoid, circular grains that are 2-5  $\mu\text{m}$  in size. Mg# in spinel displays more variance here, ranging from 95.2-99.7. Minor melilite manifests as mottled patches associated with spinel. Additionally, a rim of diopside occurs at the perimeter of FGI 7-11.

**Spinel-rich nodules:** Five spinel-rich nodules occur along the interfaces between the core and mantle of the inclusion (Fig. 4). Spinel within these nodules manifests as elongate grains that coalesce into mesh-like structures. Perovskite grains (1-2  $\mu\text{m}$  in size) are enclosed by the surrounding spinel laths. Compositions of melilite ( $\text{Åk}_{7.3-9.2}$ ) and spinel (Mg# = 99.0-99.7) within the nodules do not differ from those housed within in the core.

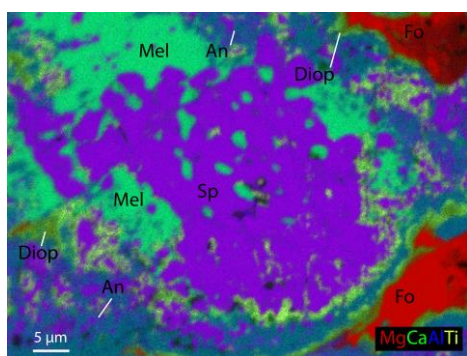


**Fig. 4.** False color x-ray map in Mg (red), Ca (green), Al (blue), and Ti (yellow) of a spinel-rich nodule from FGI 7-11.

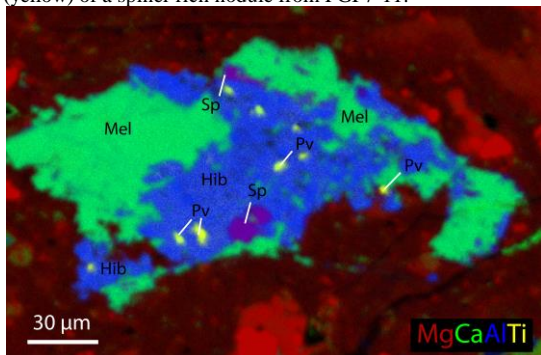


**Fig. 5.** False color x-ray map in Mg (red), Ca (green), Al (blue), and Ti (yellow) of FGI 7-10. Hib = hibanite.

**Results II. FGI 7-10** is a ~180  $\mu\text{m}$ -wide object that is composed predominantly of melilite and hibanite, with minor spinel and perovskite (Fig. 5). Spinel and perovskite grains are partially to completely enclosed by grains of hibanite, and range between 5 and 10  $\mu\text{m}$  wide. Melilite exhibits low åkermanite contents ( $\text{Åk}_{1.4-5.7}$ ), and analyses of spinel yield somewhat elevated Fe contents (Mg# = 92.1-94.4). Hibanite is relatively consistent in its chemistry, displaying a small range of compositions ( $\text{MgO} = 1.53\text{-}3.29$  wt% and  $\text{TiO}_2 = 2.89\text{-}6.83$  wt%), and yields an average stoichiometric formu-

la of  $(\text{Ca}_{0.99}\text{Mg}_{0.47}\text{Ti}_{0.47}\text{Al}_{10.93}\text{O}_{19})$ . The ratio of Mg:Ti in hibanite is consistently 1:1.

**Discussion:** Due to their fine-grained nature, anhedral crystal forms, and irregular textural features, two FGIs 7-10 and -11 from TIL 07007 studied are interpreted as the products of nebular condensation processes. Moreover, the studied CAIs vary widely in their textures and modal mineralogies, owing to a host of equally diverse formation mechanisms. In order to explain the textural and mineralogical heterogeneities observed here, we propose that these CAIs experienced separate nebular histories.

In FGI 7-11, this history is better elucidated by examining the mantle of the object. It is interpreted that the mantle is a reaction front, where melilite in the core was partially replaced by anorthite, spinel, and grossmanite [4]. The intergrowths of grossmanite and spinel in the mantle indicate that the reaction of melilite with gaseous Mg and SiO involved gaseous Ti, allowing  $\text{Ti}^{3+}$  to incorporate into pyroxene under a highly reducing condition [4]. This replacement reaction may have occurred during the formation of diopside that finally rimmed the entire inclusion.

In FGI 7-10, spinel grains are included in melilite, which indicates a deviation from the condensation sequence predicted for solids in the solar nebula [2]. Previous workers [5] have attributed this to the epitaxial nucleation of spinel over structurally similar sites in the hibanite crystal, due to a structural similarity between spinel and hibanite. Additionally, the hibanite in this inclusion appears to have undergone a reaction in which Mg and SiO gaseous phases have prompted a conversion to melilite, as predicted by [6]. Elevated Fe contents in the spinel from FGI 7-10 may indicate low-temperature parent body reworking of this object.

**Conclusions:** An examination of the evidence collected and presented within this study establishes the following outcomes: **1)** FGI 7-11 preserves evidence for a gas-solid reaction of melilite replaced by anorthite, spinel, and grossmanite. **2)** FGI 7-10 exhibits a possible crystallographic control on the nucleation and growth of spinel over hibanite. Later, melilite formed by a reaction of hibanite with gaseous Mg and SiO.

**References:** [1] MacPherson G. (2003) *Treatise on Geochemistry*. 1. 201-246. [2] Grossman L. (1972) *GCA* 36, 597-619. [3] Krot A. N. et al. (2004) *MAPS* 39, 1517-1553. [4] Han J. & Brearley A. J. (2015) *MAPS* 50, 2121-2136. [5] Han J. et al. (2015) *MAPS* 50, 2121-2136. [6] Yoneda S. & Grossman L. (1995) *GCA* 59, 3413-3444.